



Measurement of the isospin asymmetry in $B \rightarrow K^{(*)} \mu^+ \mu^-$ decays

The LHCb collaboration[†]

Abstract

The isospin asymmetries of $B \rightarrow K^{(*)} \mu^+ \mu^-$ decays and the partial branching fractions of $B^0 \rightarrow K^0 \mu^+ \mu^-$ and $B^+ \rightarrow K^{*+} \mu^+ \mu^-$ are measured as a function of the di-muon mass squared q^2 using an integrated luminosity of 1.0 fb^{-1} collected with the LHCb detector. The $B \rightarrow K \mu^+ \mu^-$ isospin asymmetry integrated over q^2 is negative, deviating from zero with over 4σ significance. The $B \rightarrow K^* \mu^+ \mu^-$ decay measurements are consistent with the Standard Model prediction of negligible isospin asymmetry. The observation of the decay $B^0 \rightarrow K_S^0 \mu^+ \mu^-$ is reported with 5.7σ significance. Assuming that the branching fraction of $B^0 \rightarrow K^0 \mu^+ \mu^-$ is twice that of $B^0 \rightarrow K_S^0 \mu^+ \mu^-$, the branching fractions of $B^0 \rightarrow K^0 \mu^+ \mu^-$ and $B \rightarrow K^{*+} \mu^+ \mu^-$ are found to be $(0.31_{-0.06}^{+0.07}) \times 10^{-6}$ and $(1.16 \pm 0.19) \times 10^{-6}$, respectively.

Submitted to Journal of High Energy Physics

[†]Authors are listed on the following pages.

LHCb collaboration

R. Aaij³⁸, C. Abellan Beteta^{33,n}, A. Adametz¹¹, B. Adeva³⁴, M. Adinolfi⁴³, C. Adrover⁶, A. Affolder⁴⁹, Z. Ajaltouni⁵, J. Albrecht³⁵, F. Alessio³⁵, M. Alexander⁴⁸, S. Ali³⁸, G. Alkhazov²⁷, P. Alvarez Cartelle³⁴, A.A. Alves Jr²², S. Amato², Y. Amhis³⁶, J. Anderson³⁷, R.B. Appleby⁵¹, O. Aquines Gutierrez¹⁰, F. Archilli^{18,35}, A. Artamonov³², M. Artuso^{53,35}, E. Aslanides⁶, G. Auriemma^{22,m}, S. Bachmann¹¹, J.J. Back⁴⁵, V. Balagura^{28,35}, W. Baldini¹⁶, R.J. Barlow⁵¹, C. Barschel³⁵, S. Barsuk⁷, W. Barter⁴⁴, A. Bates⁴⁸, C. Bauer¹⁰, Th. Bauer³⁸, A. Bay³⁶, J. Beddow⁴⁸, I. Bediaga¹, S. Belogurov²⁸, K. Belous³², I. Belyaev²⁸, E. Ben-Haim⁸, M. Benayoun⁸, G. Bencivenni¹⁸, S. Benson⁴⁷, J. Benton⁴³, R. Bernet³⁷, M.-O. Bettler¹⁷, M. van Beuzekom³⁸, A. Bien¹¹, S. Bifani¹², T. Bird⁵¹, A. Bizzeti^{17,h}, P.M. Bjørnstad⁵¹, T. Blake³⁵, F. Blanc³⁶, C. Blanks⁵⁰, J. Blouw¹¹, S. Blusk⁵³, A. Bobrov³¹, V. Bocci²², A. Bondar³¹, N. Bondar²⁷, W. Bonivento¹⁵, S. Borghi^{48,51}, A. Borgia⁵³, T.J.V. Bowcock⁴⁹, C. Bozzi¹⁶, T. Brambach⁹, J. van den Brand³⁹, J. Bressieux³⁶, D. Brett⁵¹, M. Britsch¹⁰, T. Britton⁵³, N.H. Brook⁴³, H. Brown⁴⁹, A. Büchler-Germann³⁷, I. Burducea²⁶, A. Bursche³⁷, J. Buytaert³⁵, S. Cadeddu¹⁵, O. Callot⁷, M. Calvi^{20,j}, M. Calvo Gomez^{33,n}, A. Camboni³³, P. Campana^{18,35}, A. Carbone¹⁴, G. Carboni^{21,k}, R. Cardinale^{19,i,35}, A. Cardini¹⁵, L. Carson⁵⁰, K. Carvalho Akiba², G. Casse⁴⁹, M. Cattaneo³⁵, Ch. Cauet⁹, M. Charles⁵², Ph. Charpentier³⁵, P. Chen^{3,36}, N. Chiapolini³⁷, M. Chrzaszcz²³, K. Ciba³⁵, X. Cid Vidal³⁴, G. Ciezarek⁵⁰, P.E.L. Clarke⁴⁷, M. Clemencic³⁵, H.V. Cliff⁴⁴, J. Closier³⁵, C. Coca²⁶, V. Coco³⁸, J. Cogan⁶, E. Cogneras⁵, P. Collins³⁵, A. Comerma-Montells³³, A. Contu⁵², A. Cook⁴³, M. Coombes⁴³, G. Corti³⁵, B. Couturier³⁵, G.A. Cowan³⁶, D. Craik⁴⁵, R. Currie⁴⁷, C. D'Ambrosio³⁵, P. David⁸, P.N.Y. David³⁸, I. De Bonis⁴, K. De Bruyn³⁸, S. De Capua^{21,k}, M. De Cian³⁷, J.M. De Miranda¹, L. De Paula², P. De Simone¹⁸, D. Decamp⁴, M. Deckenhoff⁹, H. Degaudenzi^{36,35}, L. Del Buono⁸, C. Deplano¹⁵, D. Derkach^{14,35}, O. Deschamps⁵, F. Dettori³⁹, J. Dickens⁴⁴, H. Dijkstra³⁵, P. Diniz Batista¹, F. Domingo Bonal^{33,n}, S. Donleavy⁴⁹, F. Dordei¹¹, A. Dosil Suárez³⁴, D. Dossett⁴⁵, A. Dovbnya⁴⁰, F. Dupertuis³⁶, R. Dzhelyadin³², A. Dziurda²³, A. Dzyuba²⁷, S. Easo⁴⁶, U. Egede⁵⁰, V. Egorychev²⁸, S. Eidelman³¹, D. van Eijk³⁸, F. Eisele¹¹, S. Eisenhardt⁴⁷, R. Ekelhof⁹, L. Eklund⁴⁸, I. El Rifai⁵, Ch. Elsasser³⁷, D. Elsby⁴², D. Esperante Pereira³⁴, A. Falabella^{16,e,14}, C. Färber¹¹, G. Fardell⁴⁷, C. Farinelli³⁸, S. Farry¹², V. Fave³⁶, V. Fernandez Albor³⁴, M. Ferro-Luzzi³⁵, S. Filippov³⁰, C. Fitzpatrick⁴⁷, M. Fontana¹⁰, F. Fontanelli^{19,i}, R. Forty³⁵, O. Francisco², M. Frank³⁵, C. Frei³⁵, M. Frosini^{17,f}, S. Furcas²⁰, A. Gallas Torreira³⁴, D. Galli^{14,c}, M. Gandelman², P. Gandini⁵², Y. Gao³, J.-C. Garnier³⁵, J. Garofoli⁵³, J. Garra Tico⁴⁴, L. Garrido³³, D. Gascon³³, C. Gaspar³⁵, R. Gauld⁵², N. Gauvin³⁶, M. Gersabeck³⁵, T. Gershon^{45,35}, Ph. Ghez⁴, V. Gibson⁴⁴, V.V. Gligorov³⁵, C. Göbel⁵⁴, D. Golubkov²⁸, A. Golutvin^{50,28,35}, A. Gomes², H. Gordon⁵², M. Grabalosa Gándara³³, R. Graciani Diaz³³, L.A. Granado Cardoso³⁵, E. Graugés³³, G. Graziani¹⁷, A. Grecu²⁶, E. Greening⁵², S. Gregson⁴⁴, O. Grünberg⁵⁵, B. Gui⁵³, E. Gushchin³⁰, Yu. Guz³², T. Gys³⁵, C. Hadjivasiliou⁵³, G. Haefeli³⁶, C. Haen³⁵, S.C. Haines⁴⁴, T. Hampson⁴³, S. Hansmann-Menzemer¹¹, N. Harnew⁵², S.T. Harnew⁴³, J. Harrison⁵¹, P.F. Harrison⁴⁵, T. Hartmann⁵⁵, J. He⁷, V. Heijne³⁸, K. Hennessy⁴⁹, P. Henrard⁵, J.A. Hernando Morata³⁴, E. van Herwijnen³⁵, E. Hicks⁴⁹, M. Hoballah⁵, P. Hopchev⁴, W. Hulsbergen³⁸, P. Hunt⁵², T. Huse⁴⁹, R.S. Huston¹², D. Hutchcroft⁴⁹, D. Hynds⁴⁸, V. Iakovenko⁴¹, P. Ilten¹², J. Imong⁴³, R. Jacobsson³⁵, A. Jaeger¹¹, M. Jahjah Hussein⁵, E. Jans³⁸, F. Jansen³⁸, P. Jaton³⁶, B. Jean-Marie⁷, F. Jing³, M. John⁵², D. Johnson⁵², C.R. Jones⁴⁴, B. Jost³⁵, M. Kaballo⁹, S. Kandybei⁴⁰, M. Karacson³⁵,

T.M. Karbach⁹, J. Keaveney¹², I.R. Kenyon⁴², U. Kerzel³⁵, T. Ketel³⁹, A. Keune³⁶,
 B. Khanji⁶, Y.M. Kim⁴⁷, M. Knecht³⁶, O. Kochebina⁷, I. Komarov²⁹, R.F. Koopman³⁹,
 P. Koppenburg³⁸, M. Korolev²⁹, A. Kozlinskiy³⁸, L. Kravchuk³⁰, K. Kreplin¹¹, M. Kreps⁴⁵,
 G. Krocker¹¹, P. Krokovny³¹, F. Kruse⁹, K. Kruzelecki³⁵, M. Kucharczyk^{20,23,35,j},
 V. Kudryavtsev³¹, T. Kvaratskheliya^{28,35}, V.N. La Thi³⁶, D. Lacarrere³⁵, G. Lafferty⁵¹,
 A. Lai¹⁵, D. Lambert⁴⁷, R.W. Lambert³⁹, E. Lanciotti³⁵, G. Lanfranchi¹⁸, C. Langenbruch³⁵,
 T. Latham⁴⁵, C. Lazzeroni⁴², R. Le Gac⁶, J. van Leerdam³⁸, J.-P. Lees⁴, R. Lefèvre⁵,
 A. Leflat^{29,35}, J. Lefrançois⁷, O. Leroy⁶, T. Lesiak²³, L. Li³, Y. Li³, L. Li Gioi⁵, M. Lieng⁹,
 M. Liles⁴⁹, R. Lindner³⁵, C. Linn¹¹, B. Liu³, G. Liu³⁵, J. von Loeben²⁰, J.H. Lopes²,
 E. Lopez Asamar³³, N. Lopez-March³⁶, H. Lu³, J. Luisier³⁶, A. Mac Raighne⁴⁸, F. Machefert⁷,
 I.V. Machikhiliyan^{4,28}, F. Maciuc¹⁰, O. Maev^{27,35}, J. Magnin¹, S. Malde⁵²,
 R.M.D. Mamunur³⁵, G. Manca^{15,d}, G. Mancinelli⁶, N. Mangiafave⁴⁴, U. Marconi¹⁴, R. Märki³⁶,
 J. Marks¹¹, G. Martellotti²², A. Martens⁸, L. Martin⁵², A. Martín Sánchez⁷, M. Martinelli³⁸,
 D. Martinez Santos³⁵, A. Massafferri¹, Z. Mathe¹², C. Matteuzzi²⁰, M. Matveev²⁷,
 E. Maurice⁶, B. Maynard⁵³, A. Mazurov^{16,30,35}, J. McCarthy⁴², G. McGregor⁵¹, R. McNulty¹²,
 M. Meissner¹¹, M. Merk³⁸, J. Merkel⁹, D.A. Milanese¹³, M.-N. Minard⁴, J. Molina Rodriguez⁵⁴,
 S. Monteil⁵, D. Moran¹², P. Morawski²³, R. Mountain⁵³, I. Mous³⁸, F. Muheim⁴⁷, K. Müller³⁷,
 R. Muresan²⁶, B. Muryn²⁴, B. Muster³⁶, J. Mylroie-Smith⁴⁹, P. Naik⁴³, T. Nakada³⁶,
 R. Nandakumar⁴⁶, I. Nasteva¹, M. Needham⁴⁷, N. Neufeld³⁵, A.D. Nguyen³⁶,
 C. Nguyen-Mau^{36,o}, M. Nicol⁷, V. Niess⁵, N. Nikitin²⁹, T. Nikodem¹¹, A. Nomerotski^{52,35},
 A. Novoselov³², A. Oblakowska-Mucha²⁴, V. Obraztsov³², S. Oggero³⁸, S. Ogilvy⁴⁸,
 O. Okhrimenko⁴¹, R. Oldeman^{15,d,35}, M. Orlandea²⁶, J.M. Otalora Goicochea², P. Owen⁵⁰,
 B.K. Pal⁵³, J. Palacios³⁷, A. Palano^{13,b}, M. Palutan¹⁸, J. Panman³⁵, A. Papanestis⁴⁶,
 M. Pappagallo⁴⁸, C. Parkes⁵¹, C.J. Parkinson⁵⁰, G. Passaleva¹⁷, G.D. Patel⁴⁹, M. Patel⁵⁰,
 G.N. Patrick⁴⁶, C. Patrignani^{19,i}, C. Pavel-Nicorescu²⁶, A. Pazos Alvarez³⁴, A. Pellegrino³⁸,
 G. Penso^{22,l}, M. Pepe Altarelli³⁵, S. Perazzini^{14,c}, D.L. Perego^{20,j}, E. Perez Trigo³⁴,
 A. Pérez-Calero Yzquierdo³³, P. Perret⁵, M. Perrin-Terrin⁶, G. Pessina²⁰, A. Petrolini^{19,i},
 A. Phan⁵³, E. Picatoste Olloqui³³, B. Pie Valls³³, B. Pietrzyk⁴, T. Pilař⁴⁵, D. Pinci²²,
 R. Plackett⁴⁸, S. Playfer⁴⁷, M. Plo Casasus³⁴, F. Polci⁸, G. Polok²³, A. Poluektov^{45,31},
 E. Polcarpo², D. Popov¹⁰, B. Popovici²⁶, C. Potterat³³, A. Powell⁵², J. Prisciandaro³⁶,
 V. Pugatch⁴¹, A. Puig Navarro³³, W. Qian⁵³, J.H. Rademacker⁴³, B. Rakotomiaramanana³⁶,
 M.S. Rangel², I. Raniuk⁴⁰, G. Raven³⁹, S. Redford⁵², M.M. Reid⁴⁵, A.C. dos Reis¹,
 S. Ricciardi⁴⁶, A. Richards⁵⁰, K. Rinnert⁴⁹, D.A. Roa Romero⁵, P. Robbe⁷, E. Rodrigues^{48,51},
 F. Rodrigues², P. Rodriguez Perez³⁴, G.J. Rogers⁴⁴, S. Roiser³⁵, V. Romanovsky³²,
 M. Rosello^{33,n}, J. Rouvinet³⁶, T. Ruf³⁵, H. Ruiz³³, G. Sabatino^{21,k}, J.J. Saborido Silva³⁴,
 N. Sagidova²⁷, P. Sail⁴⁸, B. Saitta^{15,d}, C. Salzmann³⁷, B. Sanmartin Sedes³⁴, M. Sannino^{19,i},
 R. Santacesaria²², C. Santamarina Rios³⁴, R. Santinelli³⁵, E. Santovetti^{21,k}, M. Sapunov⁶,
 A. Sarti^{18,l}, C. Satriano^{22,m}, A. Satta²¹, M. Savrie^{16,e}, D. Savrina²⁸, P. Schaack⁵⁰,
 M. Schiller³⁹, H. Schindler³⁵, S. Schleich⁹, M. Schlupp⁹, M. Schmelling¹⁰, B. Schmidt³⁵,
 O. Schneider³⁶, A. Schopper³⁵, M.-H. Schune⁷, R. Schwemmer³⁵, B. Sciascia¹⁸, A. Sciubba^{18,l},
 M. Seco³⁴, A. Semennikov²⁸, K. Senderowska²⁴, I. Sepp⁵⁰, N. Serra³⁷, J. Serrano⁶, P. Seyfert¹¹,
 M. Shapkin³², I. Shapoval^{40,35}, P. Shatalov²⁸, Y. Shcheglov²⁷, T. Shears⁴⁹, L. Shekhtman³¹,
 O. Shevchenko⁴⁰, V. Shevchenko²⁸, A. Shires⁵⁰, R. Silva Coutinho⁴⁵, T. Skwarnicki⁵³,
 N.A. Smith⁴⁹, E. Smith^{52,46}, M. Smith⁵¹, K. Sobczak⁵, F.J.P. Soler⁴⁸, A. Solomin⁴³,
 F. Soomro^{18,35}, D. Souza⁴³, B. Souza De Paula², B. Spaan⁹, A. Sparkes⁴⁷, P. Spradlin⁴⁸,
 F. Stagni³⁵, S. Stahl¹¹, O. Steinkamp³⁷, S. Stoica²⁶, S. Stone^{53,35}, B. Storaci³⁸, M. Straticiuc²⁶,

U. Straumann³⁷, V.K. Subbiah³⁵, S. Swientek⁹, M. Szczekowski²⁵, P. Szczypka³⁶,
T. Szumlak²⁴, S. T'Jampens⁴, M. Teklishyn⁷, E. Teodorescu²⁶, F. Teubert³⁵, C. Thomas⁵²,
E. Thomas³⁵, J. van Tilburg¹¹, V. Tisserand⁴, M. Tobin³⁷, S. Tol³⁹, S. Topp-Joergensen⁵²,
N. Torr⁵², E. Tournefier^{4,50}, S. Tourneur³⁶, M.T. Tran³⁶, A. Tsaregorodtsev⁶, N. Tuning³⁸,
M. Ubeda Garcia³⁵, A. Ukleja²⁵, U. Uwer¹¹, V. Vagnoni¹⁴, G. Valenti¹⁴, R. Vazquez Gomez³³,
P. Vazquez Regueiro³⁴, S. Vecchi¹⁶, J.J. Velthuis⁴³, M. Veltri^{17,9}, M. Vesterinen³⁵, B. Viaud⁷,
I. Videau⁷, D. Vieira², X. Vilasis-Cardona^{33,n}, J. Visniakov³⁴, A. Vollhardt³⁷, D. Volyanskyy¹⁰,
D. Voong⁴³, A. Vorobyev²⁷, V. Vorobyev³¹, C. Vof⁵⁵, H. Voss¹⁰, R. Waldi⁵⁵, R. Wallace¹²,
S. Wandernoth¹¹, J. Wang⁵³, D.R. Ward⁴⁴, N.K. Watson⁴², A.D. Webber⁵¹, D. Websdale⁵⁰,
M. Whitehead⁴⁵, J. Wicht³⁵, D. Wiedner¹¹, L. Wiggers³⁸, G. Wilkinson⁵², M.P. Williams^{45,46},
M. Williams⁵⁰, F.F. Wilson⁴⁶, J. Wishahi⁹, M. Witek²³, W. Witzeling³⁵, S.A. Wotton⁴⁴,
S. Wright⁴⁴, S. Wu³, K. Wyllie³⁵, Y. Xie⁴⁷, F. Xing⁵², Z. Xing⁵³, Z. Yang³, R. Young⁴⁷,
X. Yuan³, O. Yushchenko³², M. Zangoli¹⁴, M. Zavertyaev^{10,a}, F. Zhang³, L. Zhang⁵³,
W.C. Zhang¹², Y. Zhang³, A. Zhelezov¹¹, L. Zhong³, A. Zvyagin³⁵.

¹ *Centro Brasileiro de Pesquisas Físicas (CBPF), Rio de Janeiro, Brazil*

² *Universidade Federal do Rio de Janeiro (UFRJ), Rio de Janeiro, Brazil*

³ *Center for High Energy Physics, Tsinghua University, Beijing, China*

⁴ *LAPP, Université de Savoie, CNRS/IN2P3, Annecy-Le-Vieux, France*

⁵ *Clermont Université, Université Blaise Pascal, CNRS/IN2P3, LPC, Clermont-Ferrand, France*

⁶ *CPPM, Aix-Marseille Université, CNRS/IN2P3, Marseille, France*

⁷ *LAL, Université Paris-Sud, CNRS/IN2P3, Orsay, France*

⁸ *LPNHE, Université Pierre et Marie Curie, Université Paris Diderot, CNRS/IN2P3, Paris, France*

⁹ *Fakultät Physik, Technische Universität Dortmund, Dortmund, Germany*

¹⁰ *Max-Planck-Institut für Kernphysik (MPIK), Heidelberg, Germany*

¹¹ *Physikalisches Institut, Ruprecht-Karls-Universität Heidelberg, Heidelberg, Germany*

¹² *School of Physics, University College Dublin, Dublin, Ireland*

¹³ *Sezione INFN di Bari, Bari, Italy*

¹⁴ *Sezione INFN di Bologna, Bologna, Italy*

¹⁵ *Sezione INFN di Cagliari, Cagliari, Italy*

¹⁶ *Sezione INFN di Ferrara, Ferrara, Italy*

¹⁷ *Sezione INFN di Firenze, Firenze, Italy*

¹⁸ *Laboratori Nazionali dell'INFN di Frascati, Frascati, Italy*

¹⁹ *Sezione INFN di Genova, Genova, Italy*

²⁰ *Sezione INFN di Milano Bicocca, Milano, Italy*

²¹ *Sezione INFN di Roma Tor Vergata, Roma, Italy*

²² *Sezione INFN di Roma La Sapienza, Roma, Italy*

²³ *Henryk Niewodniczanski Institute of Nuclear Physics Polish Academy of Sciences, Kraków, Poland*

²⁴ *AGH University of Science and Technology, Kraków, Poland*

²⁵ *Soltan Institute for Nuclear Studies, Warsaw, Poland*

²⁶ *Horia Hulubei National Institute of Physics and Nuclear Engineering, Bucharest-Magurele, Romania*

²⁷ *Petersburg Nuclear Physics Institute (PNPI), Gatchina, Russia*

²⁸ *Institute of Theoretical and Experimental Physics (ITEP), Moscow, Russia*

²⁹ *Institute of Nuclear Physics, Moscow State University (SINP MSU), Moscow, Russia*

³⁰ *Institute for Nuclear Research of the Russian Academy of Sciences (INR RAN), Moscow, Russia*

³¹ *Budker Institute of Nuclear Physics (SB RAS) and Novosibirsk State University, Novosibirsk, Russia*

³² *Institute for High Energy Physics (IHEP), Protvino, Russia*

³³ *Universitat de Barcelona, Barcelona, Spain*

³⁴ *Universidad de Santiago de Compostela, Santiago de Compostela, Spain*

³⁵ *European Organization for Nuclear Research (CERN), Geneva, Switzerland*

- ³⁶ *Ecole Polytechnique Fédérale de Lausanne (EPFL), Lausanne, Switzerland*
- ³⁷ *Physik-Institut, Universität Zürich, Zürich, Switzerland*
- ³⁸ *Nikhef National Institute for Subatomic Physics, Amsterdam, The Netherlands*
- ³⁹ *Nikhef National Institute for Subatomic Physics and VU University Amsterdam, Amsterdam, The Netherlands*
- ⁴⁰ *NSC Kharkiv Institute of Physics and Technology (NSC KIPT), Kharkiv, Ukraine*
- ⁴¹ *Institute for Nuclear Research of the National Academy of Sciences (KINR), Kyiv, Ukraine*
- ⁴² *University of Birmingham, Birmingham, United Kingdom*
- ⁴³ *H.H. Wills Physics Laboratory, University of Bristol, Bristol, United Kingdom*
- ⁴⁴ *Cavendish Laboratory, University of Cambridge, Cambridge, United Kingdom*
- ⁴⁵ *Department of Physics, University of Warwick, Coventry, United Kingdom*
- ⁴⁶ *STFC Rutherford Appleton Laboratory, Didcot, United Kingdom*
- ⁴⁷ *School of Physics and Astronomy, University of Edinburgh, Edinburgh, United Kingdom*
- ⁴⁸ *School of Physics and Astronomy, University of Glasgow, Glasgow, United Kingdom*
- ⁴⁹ *Oliver Lodge Laboratory, University of Liverpool, Liverpool, United Kingdom*
- ⁵⁰ *Imperial College London, London, United Kingdom*
- ⁵¹ *School of Physics and Astronomy, University of Manchester, Manchester, United Kingdom*
- ⁵² *Department of Physics, University of Oxford, Oxford, United Kingdom*
- ⁵³ *Syracuse University, Syracuse, NY, United States*
- ⁵⁴ *Pontifícia Universidade Católica do Rio de Janeiro (PUC-Rio), Rio de Janeiro, Brazil, associated to ²*
- ⁵⁵ *Institut für Physik, Universität Rostock, Rostock, Germany, associated to ¹¹*
- ^a *P.N. Lebedev Physical Institute, Russian Academy of Science (LPI RAS), Moscow, Russia*
- ^b *Università di Bari, Bari, Italy*
- ^c *Università di Bologna, Bologna, Italy*
- ^d *Università di Cagliari, Cagliari, Italy*
- ^e *Università di Ferrara, Ferrara, Italy*
- ^f *Università di Firenze, Firenze, Italy*
- ^g *Università di Urbino, Urbino, Italy*
- ^h *Università di Modena e Reggio Emilia, Modena, Italy*
- ⁱ *Università di Genova, Genova, Italy*
- ^j *Università di Milano Bicocca, Milano, Italy*
- ^k *Università di Roma Tor Vergata, Roma, Italy*
- ^l *Università di Roma La Sapienza, Roma, Italy*
- ^m *Università della Basilicata, Potenza, Italy*
- ⁿ *LIFAEELS, La Salle, Universitat Ramon Llull, Barcelona, Spain*
- ^o *Hanoi University of Science, Hanoi, Viet Nam*

1 Introduction

The flavour-changing neutral current decays $B \rightarrow K^{(*)}\mu^+\mu^-$ are forbidden at tree level in the Standard Model (SM). Such transitions must proceed via loop or box diagrams and are powerful probes of physics beyond the SM. Predictions for the branching fractions of these decays suffer from relatively large uncertainties due to form factor estimates. Theoretically clean observables can be constructed from ratios or asymmetries where the leading form factor uncertainties cancel. The CP averaged isospin asymmetry (A_I) is such an observable. It is defined as

$$\begin{aligned}
 A_I &= \frac{\Gamma(B^0 \rightarrow K^{(*)0}\mu^+\mu^-) - \Gamma(B^+ \rightarrow K^{(*)+}\mu^+\mu^-)}{\Gamma(B^0 \rightarrow K^{(*)0}\mu^+\mu^-) + \Gamma(B^+ \rightarrow K^{(*)+}\mu^+\mu^-)} \\
 &= \frac{\mathcal{B}(B^0 \rightarrow K^{(*)0}\mu^+\mu^-) - \frac{\tau_0}{\tau_+}\mathcal{B}(B^+ \rightarrow K^{(*)+}\mu^+\mu^-)}{\mathcal{B}(B^0 \rightarrow K^{(*)0}\mu^+\mu^-) + \frac{\tau_0}{\tau_+}\mathcal{B}(B^+ \rightarrow K^{(*)+}\mu^+\mu^-)},
 \end{aligned} \tag{1}$$

where $\Gamma(B \rightarrow f)$ and $\mathcal{B}(B \rightarrow f)$ are the partial width and branching fraction of the $B \rightarrow f$ decay and τ_0/τ_+ is the ratio of the lifetimes of the B^0 and B^+ mesons.¹ For $B \rightarrow K^*\mu^+\mu^-$, the SM prediction for A_I is around -1% in the di-muon mass squared (q^2) region below the J/ψ resonance, apart from the very low q^2 region where it rises to $\mathcal{O}(10\%)$ as q^2 approaches zero [1]. There is no precise prediction for A_I in the $B \rightarrow K\mu^+\mu^-$ case, but it is also expected to be close to zero. The small isospin asymmetry predicted in the SM is due to initial state radiation of the spectator quark, which is different between the neutral and charged decays. Previously, A_I has been measured to be significantly below zero in the q^2 region below the J/ψ resonance [2, 3]. In particular, the combined $B \rightarrow K\mu^+\mu^-$ and $B \rightarrow K^*\mu^+\mu^-$ isospin asymmetries measured by the BaBar experiment were 3.9σ below zero. For $B \rightarrow K^*\mu^+\mu^-$, A_I is expected to be consistent with the $B \rightarrow K^{*0}\gamma$ measurement of $5 \pm 3\%$ [4] as q^2 approaches zero. No such constraint is present for $B \rightarrow K\mu^+\mu^-$.

The isospin asymmetries are determined by measuring the differential branching fractions of $B^+ \rightarrow K^+\mu^+\mu^-$, $B^0 \rightarrow K_s^0\mu^+\mu^-$, $B^0 \rightarrow (K^{*0} \rightarrow K^+\pi^-)\mu^+\mu^-$ and $B^+ \rightarrow (K^{*+} \rightarrow K_s^0\pi^+)\mu^+\mu^-$; the decays involving a K_L^0 or π^0 are not considered. The K_s^0 meson is reconstructed via the $K_s^0 \rightarrow \pi^+\pi^-$ decay mode. The signal selections (Section 3) are optimised to provide the lowest overall uncertainty on the isospin asymmetries; this leads to a very tight selection for the $B^+ \rightarrow K^+\mu^+\mu^-$ and $B^0 \rightarrow (K^{*0} \rightarrow K^+\pi^-)\mu^+\mu^-$ channels where signal yield is sacrificed to achieve overall uniformity with the $B^0 \rightarrow K_s^0\mu^+\mu^-$ and $B^+ \rightarrow (K^{*+} \rightarrow K_s^0\pi^+)\mu^+\mu^-$ channels, respectively. In order to convert a signal yield into a branching fraction, the four signal channels are normalised to the corresponding $B \rightarrow J/\psi K^{(*)}$ channels (Section 5). The relative normalisation in each q^2 bin is performed by calculating the relative efficiency between the signal and normalisation channels using simulated events. The normalisation of $B^0 \rightarrow K^0\mu^+\mu^-$ assumes that $\mathcal{B}(B^0 \rightarrow K^0\mu^+\mu^-) = 2\mathcal{B}(B^0 \rightarrow K_s^0\mu^+\mu^-)$. Finally, A_I is determined by simultaneously fitting the $K^{(*)}\mu^+\mu^-$ mass distributions for all signal channels. Confidence

¹Charge conjugation is implied throughout this paper.

35 intervals are estimated for A_{Γ} using a profile likelihood method (Section 7). Systematic
36 uncertainties are included in the fit using Gaussian constraints.

37 **2 Experimental setup**

38 The measurements described in this paper are performed with 1.0 fb^{-1} of pp collision data
39 collected with the LHCb detector at the CERN LHC during 2011. The LHCb detector [5]
40 is a single-arm forward spectrometer covering the pseudorapidity range $2 < \eta < 5$, de-
41 signed for the study of particles containing b or c quarks. The detector includes a high
42 precision tracking system consisting of a silicon-strip vertex detector (VELO) surrounding
43 the pp interaction region, a large-area silicon-strip detector (TT) located upstream of a
44 dipole magnet with a bending power of about 4 Tm , and three stations of silicon-strip
45 detectors and straw drift-tubes placed downstream. The combined tracking system has a
46 momentum resolution $\Delta p/p$ that varies from 0.4% at $5 \text{ GeV}/c$ to 0.6% at $100 \text{ GeV}/c$, and
47 an impact parameter (IP) resolution of $20 \text{ }\mu\text{m}$ for tracks with high transverse momentum.
48 Charged hadrons are identified using two ring-imaging Cherenkov (RICH) detectors. Pho-
49 ton, electron and hadron candidates are identified by a calorimeter system consisting of
50 scintillating-pad and pre-shower detectors, an electromagnetic calorimeter and a hadronic
51 calorimeter. Muons are identified by a muon system composed of alternating layers of
52 iron and multiwire proportional chambers.

53 The trigger consists of a hardware stage, based on information from the calorimeter
54 and muon systems, followed by a software stage which applies a full event reconstruction.
55 For this analysis, candidate events are first required to pass a hardware trigger which
56 selects muons with a transverse momentum, $p_{\text{T}} > 1.48 \text{ GeV}/c$ for one muon, and 0.56 and
57 $0.48 \text{ GeV}/c$ for two muons. In the subsequent software trigger [6], at least one of the final
58 state particles is required to have both $p_{\text{T}} > 0.8 \text{ GeV}/c$ and $\text{IP} > 100 \text{ }\mu\text{m}$ with respect to
59 all of the primary proton-proton interaction vertices in the event. Finally, the tracks of
60 two or more of the final state particles are required to form a vertex which is significantly
61 displaced from the primary vertices in the event.

62 For the simulation, pp collisions are generated using PYTHIA 6.4 [7] with a specific
63 LHCb configuration [8]. Decays of hadronic particles are described by EVTGEN [9] in
64 which final state radiation is generated using PHOTOS [10]. The EVTGEN physics model
65 used is based on Ref. [11]. The interaction of the generated particles with the detector
66 and its response are implemented using the GEANT4 toolkit [12] as described in Ref. [13].

67 **3 Event selection**

68 Candidates are reconstructed with an initial cut-based selection, which is designed to
69 reduce the dataset to a manageable level. Channels involving a K_{s}^0 meson are referred
70 to as K_{s}^0 channels whereas those with a K^+ meson are referred to as K^+ channels.
71 Only events which are triggered independently of the K^+ candidate are accepted.
72 Therefore, apart from a small contribution from candidates which are triggered by the

73 K_s^0 meson, the K_s^0 and the K^+ channels are triggered in a similar way. The initial
 74 selection places requirements on the geometry, kinematics and particle identification
 75 (PID) information of the signal candidates. Kaons are identified using information from
 76 the RICH detectors, such as the difference in log-likelihood (DLL) between the kaon
 77 and pion hypothesis, $DLL_{K\pi}$. Kaon candidates are required to have $DLL_{K\pi} > 1$, which
 78 has a kaon efficiency of $\sim 85\%$ and a pion efficiency of $\sim 10\%$. Muons are identified
 79 using the amount of hits in the muon stations combined with information from the
 80 calorimeter and RICH systems. The muon PID efficiency is around 90%. Candidate
 81 K_s^0 are required to have a di-pion mass within 30 MeV/ c^2 of the nominal K_s^0 mass
 82 and K^* candidates are required to have an mass within 100 MeV/ c^2 of the nominal K^*
 83 mass. At this stage, the K_s^0 channels are split into two categories depending on how
 84 the pions from the K_s^0 decay are reconstructed. For decays where both pions have hits
 85 inside the VELO and the downstream tracking detectors the K_s^0 candidates are classified
 86 as long (L). If the daughter pions are reconstructed without VELO hits (but still with
 87 TT hits upstream of the magnet) they are classified as downstream (D) K_s^0 candidates.
 88 Separate selections are applied to the L and D categories in order to maximise the
 89 sensitivity. The selection criteria described in the next paragraph refer to the K_s^0 channels.

90
 91 After the initial selection, the L category has a much lower level of background than
 92 the D category. For this reason simple cut-based selections are applied to the former,
 93 whereas multivariate selections are employed for the latter. Both B^0 and B^+ L selections
 94 require the K_s^0 decay time to be greater than 3 ps, and for the IP χ^2 to be greater than 10
 95 when the IP of the K_s^0 , with respect to the PV, is forced to be zero. The $B^0 \rightarrow K^0 \mu^+ \mu^-$
 96 L selection requires that $K_s^0 p_T > 1$ GeV/ c and $B p_T > 2$ GeV/ c . The K_s^0 mass window is
 97 also tightened to ± 20 MeV/ c^2 . The $B^+ \rightarrow K^{*+} \mu^+ \mu^-$ L selection requires that the pion from
 98 the K^{*+} has an IP $\chi^2 > 30$. Multi-variate selections are applied to the D categories using
 99 a boosted decision tree (BDT) [14] which uses geometrical and kinematic information of
 100 the B candidate and of its daughters. The most discriminating variables according to
 101 the B^0 and B^+ BDTs are the $K_s^0 p_T$ and the angle between the B momentum and its
 102 line of flight (from the primary vertex to the decay vertex). The BDTs are trained and
 103 tested on simulated events for the signal and data for the background. The simulated
 104 events have been corrected to match the data as described in Sect. 5. All the variables
 105 used in the BDTs are well described in the simulation after correction. The background
 106 sample used is 25% of B candidates which have $|m_{K^{(*)}\mu^+\mu^-} - m_B| > 60$ MeV/ c^2 , where
 107 m_B is obtained from fits to the appropriate $B \rightarrow J/\psi K^{(*)}$ normalisation channel. These
 108 data are excluded from the analysis. The selection based on the BDT output maximises
 109 the metric $S/\sqrt{S+B}$, where S and B are the expected signal and background yields,
 110 respectively.

111 The K^+ channels have, as far as possible, the same selection criteria as used to select
 112 the K_s^0 channels. The cut-based selections applied to the L categories have the K_s^0 specific
 113 variables (e.g. K_s^0 decay time) removed and the remaining requirements are applied to
 114 the K^+ channels. The BDTs trained on the D categories contain variables which can be
 115 applied to both K_s^0 and K^+ candidates and the BDTs trained on the K_s^0 channels are

116 simply applied to the corresponding K^+ channels. The K^+ channels are therefore also
 117 split into two different categories, one of which has the L selection applied, while the other
 118 one has the D selection applied. The overlap of events between these categories induces
 119 a correlation between the L and D categories for the K^+ channels. This correlation is
 120 accounted for in the fit to A_1 .

121 The final selection reduces the combinatorial background remaining after the initial
 122 selection by a factor of 5–20, while retaining 60–90% of the signal, depending on the cat-
 123 egory and decay mode. It is ineffective at reducing background from fully reconstructed
 124 B decays, where one or more final state particles have been misidentified. Additional
 125 selection criteria are therefore applied. For the K_s^0 channels, the $\Lambda \rightarrow p\pi^-$ decay can be
 126 mistaken for a $K_s^0 \rightarrow \pi^+\pi^-$ decay if the proton is misidentified as a pion. If one of the
 127 pion daughters from the K_s^0 candidate has a $DLL_{p\pi} > 10$, the proton mass hypothesis is
 128 assigned to it. For the L(D) categories, if the $p\pi^-$ mass is within 10(15) MeV/c^2 of the
 129 nominal Λ mass the candidate is rejected. This selection eliminates background from
 130 $\Lambda_b^0 \rightarrow (\Lambda \rightarrow p\pi^-)\mu^+\mu^-$ which peaks above the B mass. For the $B^0 \rightarrow K^{*0}\mu^+\mu^-$ decay, the
 131 same peaking background vetoes are used as in Ref. [15], which remove contaminations
 132 from $B_s^0 \rightarrow \phi\mu^+\mu^-$, $B^0 \rightarrow J/\psi K^{*0}$ and $B^0 \rightarrow K^{*0}\mu^+\mu^-$ decays where the kaon and pion
 133 are swapped. Finally, for the $B^+ \rightarrow K^+\mu^+\mu^-$ decay, backgrounds from $B^+ \rightarrow J/\psi K^+$
 134 and $B \rightarrow \psi(2S)K^+$ are present, where the K^+ and μ^+ candidates are swapped. If a
 135 candidate has a $K^+\mu^-$ track combination consistent with originating from a J/ψ or
 136 $\psi(2S)$ resonance, the kaon is required to be inside the acceptance of the muon system
 137 but to have insufficient hits in the muon stations to be classified as a muon. These vetoes
 138 remove less than 1% of the signal and reduce peaking backgrounds to a negligible level.

139
 140 The mass distribution of B candidates is shown versus the di-muon mass for $B^+ \rightarrow$
 141 $K^+\mu^+\mu^-$ data in Fig. 1. The other signal channels have similar distributions, but with
 142 a smaller number of events. The excess of candidates seen as horizontal bands around
 143 3090 MeV/c^2 and 3690 MeV/c^2 are due to J/ψ and $\psi(2S)$ decays, respectively. These
 144 events are removed from the signal channels by excluding the di-muon regions in the
 145 ranges 2946–3181 MeV/c^2 and 3586–3766 MeV/c^2 . If a B candidate has an mass below
 146 5220 MeV/c^2 the veto is extended to 2800–3181 MeV/c^2 and 3450–3766 MeV/c^2 to elim-
 147 inate candidates for which the J/ψ or the $\psi(2S)$ decay undergoes final state radiation.
 148 Such events are shown in Fig. 1 as regions (a). In a small fraction of events, the di-muon
 149 mass is poorly reconstructed. This causes the J/ψ and $\psi(2S)$ decay to leak into the re-
 150 gion just above the B mass. These events are shown in Fig. 1 as regions (b). The veto
 151 is extended to 2946–3250 MeV/c^2 and 3586–3816 MeV/c^2 in the candidate B mass region
 152 from 5330–5460 MeV/c^2 to eliminate these events. These vetoes largely remove the char-
 153 monium resonances and reduce the combinatorial background. Regions (c) in Fig. 1 are
 154 composed of $B \rightarrow J/\psi K^+ X$ and $B \rightarrow \psi(2S)K^+ X$ decays where X is not reconstructed.
 155 In the subsequent analysis only candidates with masses above 5170 MeV/c^2 are included
 156 to avoid dependence on the shape of this background.

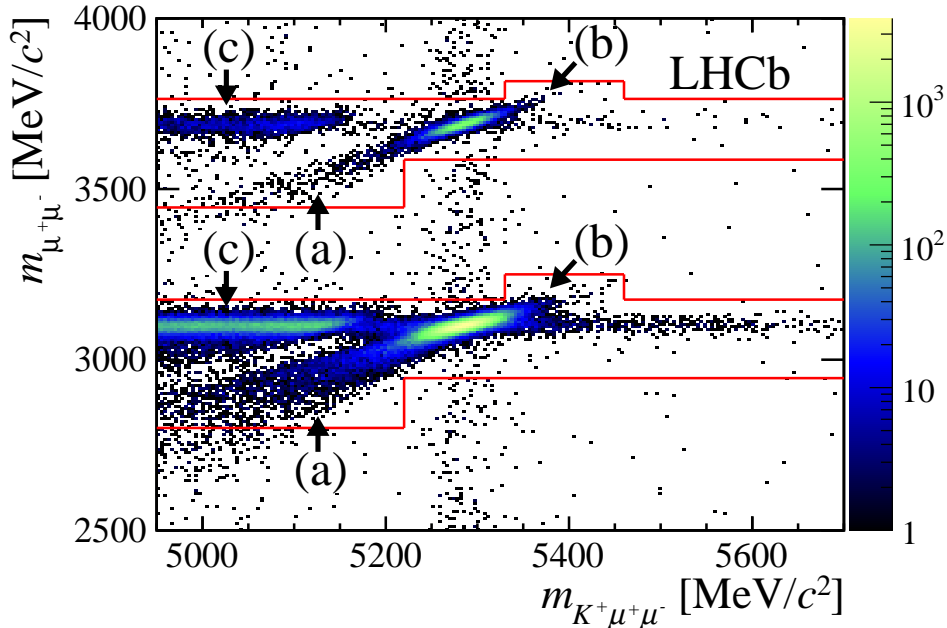


Figure 1: Mass of the di-muon versus the mass of the $B^+ \rightarrow K^+\mu^+\mu^-$ candidates. Only the di-muon mass region close to the J/ψ and $\psi(2S)$ masses is shown. The lines show the boundaries of the regions which are removed. Regions (a)–(c) are explained in the text.

Table 1: Signal yields of the $B \rightarrow K^{(*)}\mu^+\mu^-$ decays. The upper bound of the highest q^2 bin, q_{\max}^2 , is $19.3 \text{ GeV}^2/c^4$ and $23.0 \text{ GeV}^2/c^4$ for $B \rightarrow K^*\mu^+\mu^-$ and $B \rightarrow K\mu^+\mu^-$, respectively.

q^2 range [GeV^2/c^4]	$K_s^0\mu^+\mu^-$		$K^+\mu^+\mu^-$	$K^{*+}\mu^+\mu^-$		$K^{*0}\mu^+\mu^-$
	L	D	L + D	L	D	L + D
0.05 – 2.00	1 ± 2	2 ± 3	135 ± 13	4 ± 3	5 ± 4	108 ± 11
2.00 – 4.30	2 ± 3	-1 ± 3	175 ± 16	3 ± 2	5 ± 3	53 ± 9
4.30 – 8.68	9 ± 4	16 ± 6	303 ± 22	4 ± 3	17 ± 6	203 ± 17
10.09 – 12.86	4 ± 3	10 ± 4	214 ± 18	4 ± 3	15 ± 5	128 ± 14
14.18 – 16.00	3 ± 2	3 ± 3	166 ± 15	5 ± 3	4 ± 3	90 ± 10
16.00 – q_{\max}^2	5 ± 3	4 ± 3	257 ± 19	2 ± 1	4 ± 3	80 ± 11
1.00 – 6.00	8 ± 4	3 ± 6	356 ± 23	5 ± 3	15 ± 5	155 ± 15
0.05 – q_{\max}^2	25 ± 8	35 ± 11	1250 ± 42	23 ± 6	53 ± 10	673 ± 30

157 4 Signal yield determination

158 The yields for the signal channels are determined using extended unbinned maximum like-
159 likelihood fits to the $K^{(*)}\mu^+\mu^-$ mass in the range 5170–5700 MeV/c^2 . These fits are performed

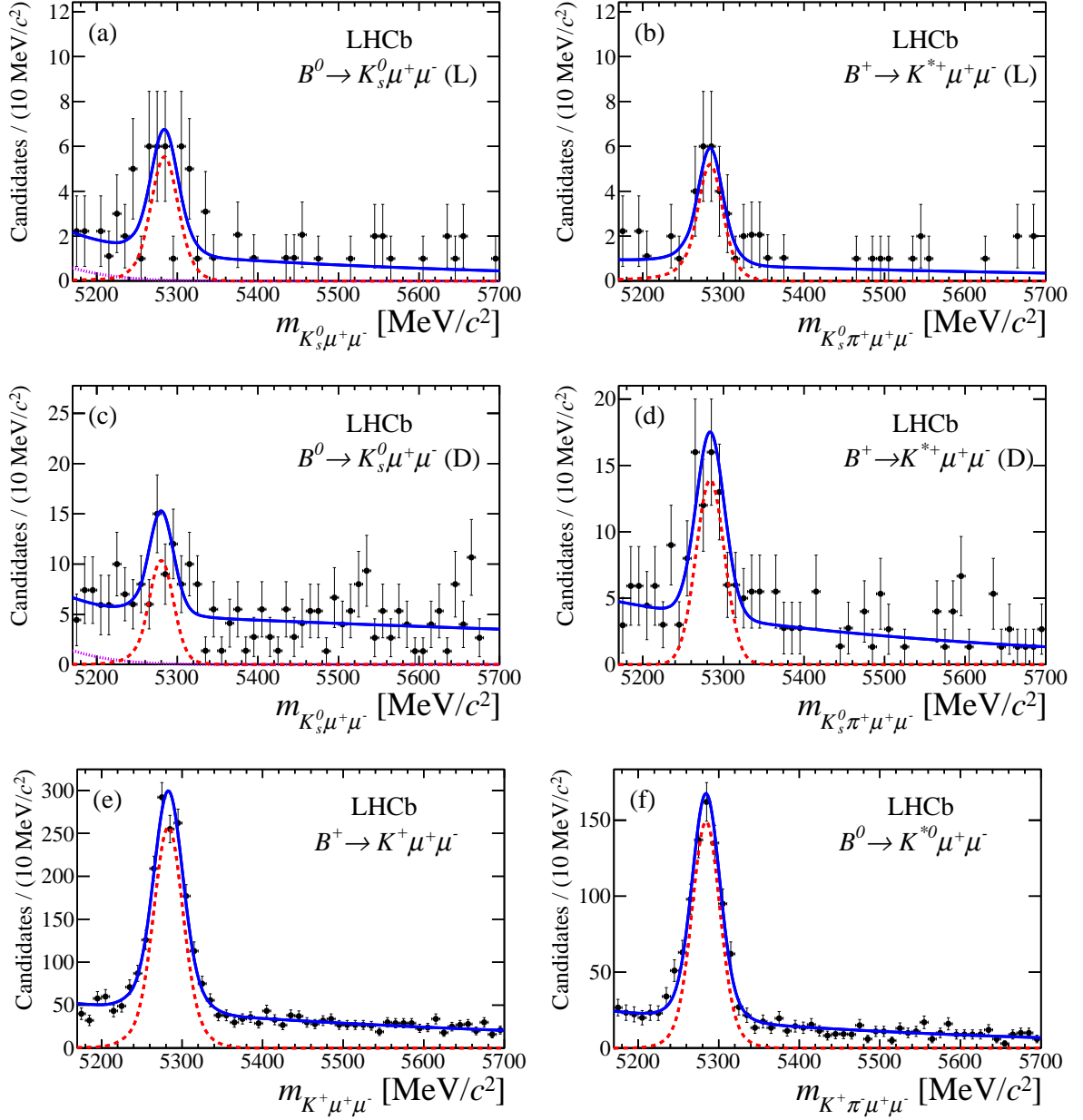


Figure 2: Mass distributions and fits of the signal channels integrated over the full q^2 region. For the K_s^0 channels, the plots are shown separately for the L and D K_s^0 reconstruction categories, (a,b) and (c,d) respectively. The signal component is shown by the dashed line, the partially reconstructed component in 2(a) and 2(c) is shown by the dotted line while the solid line shows the entire fit model.

160 in seven q^2 bins and over the full range as shown in Table 1. The results of the fits inte-
 161 grated over the full q^2 range are shown in Fig. 2. After selection, the mass of K_s^0 candidates
 162 is constrained to the nominal K_s^0 mass. The signal component is described by the sum

163 of two Crystal Ball functions [16] with common peak and tail parameters, but different
 164 widths. The shape is taken to be the same as the $B \rightarrow J/\psi K^{(*)}$ normalisation channels.
 165 The combinatorial background is fitted with a single exponential function. As stated
 166 in Sect. 3, part of the combinatorial background is removed by the charmonium vetoes.
 167 This is accounted for by scaling the remaining background. For the $B \rightarrow K\mu^+\mu^-$ decays,
 168 a component arising mainly from partially reconstructed $B \rightarrow K^*\mu^+\mu^-$ decays is present
 169 at masses below the B mass. This partially reconstructed background is characterised
 170 using a threshold model detailed in Ref. [17]. The shape of the partial reconstruction
 171 component is again assumed to be the same as for the normalisation channels. For the
 172 $B^+ \rightarrow K^+\mu^+\mu^-$ channel, the impact of this component is negligible due to the relatively
 173 high signal and low background yields. For the $B^0 \rightarrow K_s^0\mu^+\mu^-$ channel, the amount of
 174 partially reconstructed decays is found to be less than 25% of the total combinatorial
 175 background in the fit range.

176 The signal-shape parameters are allowed to vary in the $B^0 \rightarrow J/\psi K_s^0$ mass fits
 177 and are subsequently fixed for the $B^0 \rightarrow K_s^0\mu^+\mu^-$ mass fits when calculating the
 178 significance. The significance σ of a signal S for $B^0 \rightarrow K_s^0\mu^+\mu^-$ is defined as
 179 $\sigma^2 = 2\ln\mathcal{L}^L(S) + 2\ln\mathcal{L}^D(S) - 2\ln\mathcal{L}^L(0) - 2\ln\mathcal{L}^D(0)$ where $\mathcal{L}^{L,D}(S)$ and $\mathcal{L}^{L,D}(0)$ are the
 180 likelihoods of the fit with and without the signal component, respectively. The
 181 $B^0 \rightarrow K_s^0\mu^+\mu^-$ channel is observed with a significance of 5.7σ .

182 5 Normalisation

183 In order to simplify the calculation of systematic uncertainties, each signal mode is nor-
 184 malised to the $B \rightarrow J/\psi K^{(*)}$ channel, where the J/ψ decays into two muons. These decays
 185 have well measured branching fractions which are approximately two orders of magnitude
 186 higher than those of the signal decays. Each normalisation channel has similar kinematics
 187 and the same final state particles as the signal modes.

188 The relative efficiency between signal and normalisation channels is estimated using
 189 simulated events. After smearing the IP resolution of all tracks by 20%, the IP distribu-
 190 tions of candidates in the simulation and data agree well. The performance of the PID is
 191 studied using the decay $D^{*+} \rightarrow (D^0 \rightarrow \pi^+K^-)\pi^+$, which provides a clean source of kaons
 192 to study the kaon PID efficiency, and a *tag-and-probe* sample of $B^+ \rightarrow J/\psi K^+$ to study
 193 the muon PID efficiency. The simulation is reweighted to match the PID performance of
 194 the data.

195 Integrating over q^2 , the relative efficiency between the signal and normalisation chan-
 196 nels is between 70 and 80% depending on the decay mode and category. The relative
 197 efficiency includes differences in the geometrical acceptance, as well as the reconstruction,
 198 selection and trigger efficiencies. Most of these effects cancel in the efficiency ratio be-
 199 tween K_s^0 and K^+ channels, as shown in Fig. 3. The dominant effect remaining is due
 200 to the K_s^0 reconstruction efficiency, which depends on the K_s^0 momentum. At low q^2 , the
 201 efficiency for $B^0 \rightarrow K_s^0\mu^+\mu^-$ (D) decreases with respect to that for $B^+ \rightarrow K^+\mu^+\mu^-$ due to
 202 the high K_s^0 momentum in this region. This results in the K_s^0 meson more often decaying

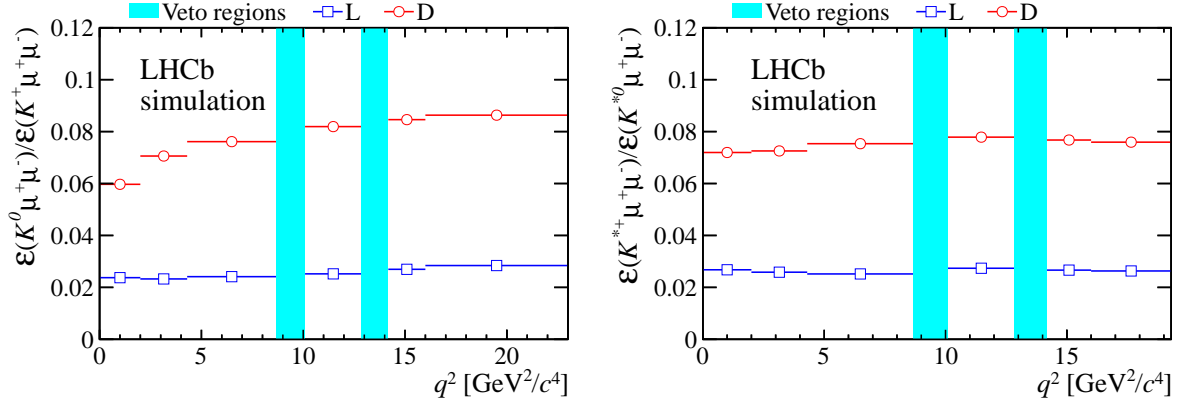


Figure 3: Efficiency of the K_s^0 channels with respect to the K^+ channels for (left) $B \rightarrow K \mu^+ \mu^-$ and (right) $B \rightarrow K^* \mu^+ \mu^-$, calculated using the simulation. The efficiencies are shown for both L and D K_s^0 reconstruction categories and include the visible branching fraction of $K^0 \rightarrow K_s^0 \rightarrow \pi^+ \pi^-$. The error bars are not visible as they are smaller than the marker size.

203 beyond the TT and consequently it has a lower reconstruction efficiency. This effect is
 204 not seen in the $B^+ \rightarrow K^{*+} \mu^+ \mu^-$ D category as the K_s^0 typically has lower momentum in
 205 this decay and so the K_s^0 reconstruction efficiency is approximately constant across q^2 .
 206 This K_s^0 reconstruction effect is also seen in the L category for both modes but is par-
 207 tially compensated by the fact that the K_s^0 daughters can cause the event to be triggered,
 208 which increases the trigger efficiency with respect to the K^+ channels at low q^2 . Summed
 209 over both the L and D categories, the efficiency of the decays involving a K^0 meson is
 210 approximately 10% with respect to those involving a charged kaon. This is partly due to
 211 the visible branching fraction of $K^0 \rightarrow K_s^0 \rightarrow \pi^+ \pi^-$ ($\sim 30\%$) and partly due to the lower
 212 reconstruction efficiency of the K_s^0 due to the long lifetime and the need to reconstruct an
 213 additional track ($\sim 30\%$). The relative efficiency between the L and D signal categories is
 214 cross-checked by comparing the ratio for the $B \rightarrow \psi(2S) K^{(*)}$ decay to the corresponding
 215 ratio for the $B \rightarrow J/\psi K^{(*)}$ decays seen in data. The results agree within the statistical
 216 accuracy of 5%.

217 6 Systematic uncertainties

218 Gaussian constraints are used to include all systematic uncertainties in the fits for A_1
 219 and the branching fractions. In most cases the dominant systematic uncertainty is that
 220 from the branching fraction measurements of the normalisation channels, ranging from 3
 221 to 6%. There is also a statistical uncertainty on the yield of the normalisation channels,
 222 which is in the range 0.5–2.0%, depending on the channel.

223 The finite size of the simulation samples introduces a statistical uncertainty on the
 224 relative efficiency and leads to a systematic uncertainty in the range 0.8–2.5% depending

225 on q^2 and decay mode.

226 The relative tracking efficiency between the signal and normalisation channels is cor-
227 rected using data. The statistical precision of these corrections leads to a systematic
228 uncertainty of $\sim 0.2\%$ per long track. The differences between the downstream tracking
229 efficiency between the simulation and data are expected to mostly cancel in the normal-
230 isation procedure. A conservative systematic uncertainty of 1% per downstream track is
231 assigned for the variation across q^2 .

232 The PID efficiency is derived from data, and its corresponding systematic uncertainty
233 arises from the statistical error associated with the PID efficiency measurements. The
234 uncertainty on the relative efficiency is determined by randomly varying PID efficiencies
235 within their uncertainties, and recomputing the relative efficiency. The resulting uncer-
236 tainty is found to be negligible.

237 The trigger efficiency is calculated using the simulation. Its uncertainty consists of
238 two components, one associated with the trigger efficiency of the K_s^0 meson, and one
239 associated with the trigger efficiency of the muons (and pion from the K^*). For the
240 muons and pion the uncertainty is obtained using $B^+ \rightarrow J/\psi K^+$ and $B^0 \rightarrow J/\psi K^{*0}$
241 events in data that are triggered independently of the signal. These candidates are used
242 to calculate the trigger efficiency and are compared to the efficiency calculated using the
243 same method in simulation. The difference is found to be $\sim 2\%$ for both $B^+ \rightarrow J/\psi K^+$
244 and $B^0 \rightarrow J/\psi K^{*0}$ decays and is assigned as a systematic uncertainty. This uncertainty is
245 assumed to cancel for the isospin asymmetry as the presence of muons is common between
246 the K_s^0 channels and the K^+ channels. The uncertainty associated with the K_s^0 trigger
247 efficiency is calculated by comparing the fraction of candidates triggered by K_s^0 daughters
248 in the simulation and the data. The difference is used as an estimate of the capability of
249 simulation to reproduce these trigger decisions. The simulation is found to underestimate
250 the K_s^0 trigger decisions by $10\text{--}20\%$ depending on the decay mode. This percentage is
251 multiplied by the fraction of trigger decisions where the K_s^0 participates in a given bin of
252 q^2 leading to an uncertainty of $0.2\text{--}4.1\%$ depending on q^2 and decay mode.

253 The effect of the unknown angular distribution of $B^+ \rightarrow K^{*+}\mu^+\mu^-$ decays on the
254 relative efficiency is estimated by altering the Wilson coefficients appearing in the operator
255 product expansion method [18, 19]. The Wilson coefficients, \mathcal{C}_7 and \mathcal{C}_{10} , have their real
256 part inverted and the relative efficiency is recalculated. This can be seen as an extreme
257 variation which is used to obtain a conservative estimate of the associated uncertainty.
258 The calculation was performed using an EVTGEN physics model which uses the transition
259 form factors detailed in Ref. [20]. The difference in the relative efficiency varies from $0\text{--}6\%$,
260 depending on q^2 , and it is assigned as a systematic uncertainty.

261 The shape parameters for the signal modes are assumed to be the same as the nor-
262 malisation channels. This assumption is validated using the simulation and no systematic
263 uncertainty is assigned. The statistical uncertainties of these shape parameters are prop-
264 agated through the fit using Gaussian constraints, accounting for correlations between
265 the parameters. The uncertainty on the amount of partially reconstructed background
266 is also added to the fit using Gaussian constraints, therefore no further uncertainty is
267 added. The parametrisation of the fit model is cross-checked by varying the fit range

268 and background model. Consistent yields are observed and no systematic uncertainty is
 269 assigned.

270 Overall the systematic error on the branching fraction is 4–8% depending on q^2 and
 271 the decay mode. This is small compared to the typical statistical error of $\sim 40\%$.

272 7 Results and conclusions

273 The differential branching fraction in the i^{th} q^2 bin can be written as

$$\frac{d\mathcal{B}^i}{dq^2} = \frac{N^i(B \rightarrow K^{(*)}\mu^+\mu^-)}{N(B \rightarrow J/\psi K^{(*)})} \times \frac{\mathcal{B}(B \rightarrow J/\psi K^{(*)})\mathcal{B}(J/\psi \rightarrow \mu^+\mu^-)}{\epsilon_{\text{rel}}^i \Delta^i}, \quad (2)$$

274 where $N^i(B \rightarrow K^{(*)}\mu^+\mu^-)$ is the number of signal candidates in bin i , $N(B \rightarrow J/\psi K^{(*)})$
 275 is the number of normalisation candidates, the product of $\mathcal{B}(B \rightarrow J/\psi K^{(*)})$ and
 276 $\mathcal{B}(J/\psi \rightarrow \mu^+\mu^-)$ is the visible branching fraction of the normalisation channel [21], ϵ_{rel}^i is
 277 the relative efficiency between the signal and normalisation channels in bin i and finally
 278 Δ^i is the bin i width. The differential branching fraction is determined by simultane-
 279 ously fitting the L and D categories of the signal channels. The branching fraction of
 280 the signal channel is introduced as a fit parameter by re-arranging Eq. (2) in terms of
 281 $N(B \rightarrow K^{(*)}\mu^+\mu^-)$. Confidence intervals are evaluated by scanning the profile likelihood.
 282 The results of these fits for $B^0 \rightarrow K^0\mu^+\mu^-$ and $B^+ \rightarrow K^{*+}\mu^+\mu^-$ decays are shown in
 283 Fig. 4 and given in Tables 2 and 3. Theoretical predictions [22, 23, 24] are superimposed
 284 on Figs. 4 and 5. In the low q^2 region, these predictions rely on the QCD factorisation
 285 approaches from Refs. [25, 26] for $B \rightarrow K^*\mu^+\mu^-$ and Ref. [27] for $B \rightarrow K\mu^+\mu^-$ which lose
 286 accuracy when approaching the J/ψ resonance. In the high q^2 region, an operator product
 287 expansion in the inverse b -quark mass, $1/m_b$, and in $1/\sqrt{q^2}$ is used based on Ref. [28].
 288 This expansion is only valid above the open charm threshold. In both q^2 regions the
 289 form factor calculations for $B \rightarrow K^*\mu^+\mu^-$ and $B \rightarrow K\mu^+\mu^-$ are taken from Refs. [29]
 290 and [30] respectively. These form factors lead to a high correlation in the uncertainty
 291 of the predictions across q^2 . A dimensional estimate is made of the uncertainty from
 292 expansion corrections [31]. The non-zero isospin asymmetry arises in the low q^2 region
 293 due to spectator-quark differences in the so-called hard-scattering part. There are also
 294 sub-leading corrections included from Refs. [1] and [26] which only affect the charged
 295 modes and further contribute to the isospin asymmetry.

296 The total branching fractions are also measured by extrapolating underneath the char-
 297 monium resonances assuming the same q^2 distribution as in the simulation. The branching
 298 fractions of $B^0 \rightarrow K^0\mu^+\mu^-$ and $B^+ \rightarrow K^{*+}\mu^+\mu^-$ are found to be

$$\begin{aligned} \mathcal{B}(B^0 \rightarrow K^0\mu^+\mu^-) &= (0.31_{-0.06}^{+0.07}) \times 10^{-6} \quad \text{and} \\ \mathcal{B}(B^+ \rightarrow K^{*+}\mu^+\mu^-) &= (1.16 \pm 0.19) \times 10^{-6}, \end{aligned}$$

299 respectively, where the errors include statistical and systematic uncertainties. These re-
 300 sults are in agreement with previous measurements and with better precision [21].

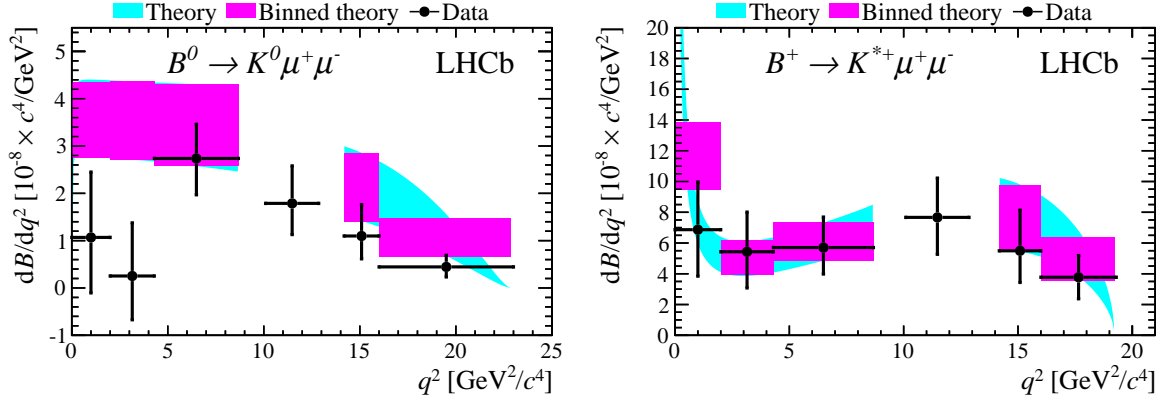


Figure 4: Differential branching fractions of (left) $B^0 \rightarrow K^0 \mu^+ \mu^-$ and (right) $B^+ \rightarrow K^{*+} \mu^+ \mu^-$. The theoretical SM predictions are taken from Refs. [22, 23].

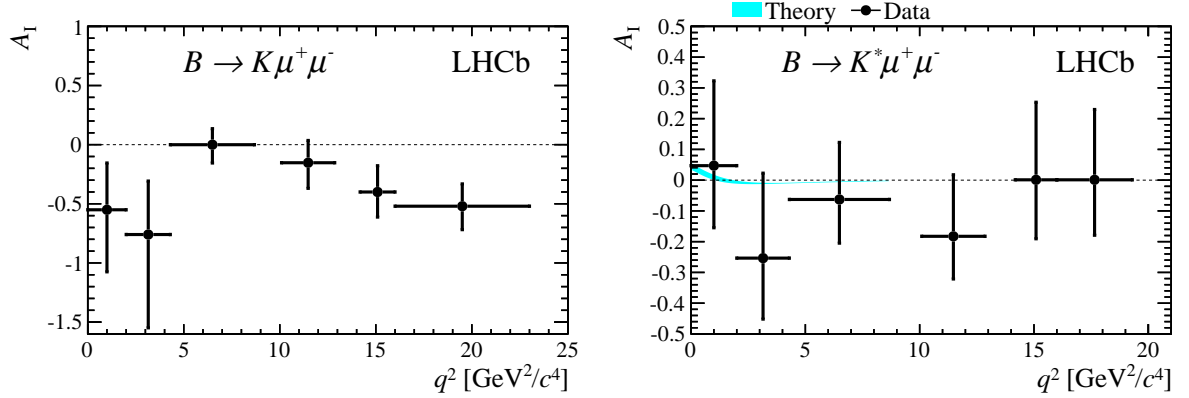


Figure 5: Isospin asymmetry of (left) $B \rightarrow K \mu^+ \mu^-$ and (right) $B \rightarrow K^* \mu^+ \mu^-$. For $B \rightarrow K^* \mu^+ \mu^-$ the theoretical SM prediction, which is very close to zero, is shown for q^2 below $8.68 \text{ GeV}^2/c^2$, from Ref. [24].

301 The isospin asymmetries as a function of q^2 for $B \rightarrow K \mu^+ \mu^-$ and $B \rightarrow K^* \mu^+ \mu^-$ are
 302 shown in Fig. 5 and given in Tables 2 and 3. As for the branching fractions, the fit is done
 303 simultaneously for both the L and D categories where A_I is a common parameter for the
 304 two cases. The confidence intervals are also determined by scanning the profile likelihood.
 305 The significance of the deviation from the null hypothesis is obtained by fixing A_I to be
 306 zero and computing the difference in the negative log-likelihood from the nominal fit.

307 In summary, the isospin asymmetries of $B \rightarrow K^{(*)} \mu^+ \mu^-$ decays and the branching
 308 fractions of $B^0 \rightarrow K^0 \mu^+ \mu^-$ and $B^+ \rightarrow K^{*+} \mu^+ \mu^-$ are measured, using 1.0 fb^{-1} of data taken
 309 with the LHCb detector. The two q^2 bins below $4.3 \text{ GeV}^2/c^2$ and the highest bin above
 310 $16 \text{ GeV}^2/c^2$ have the most negative isospin asymmetry in the $B \rightarrow K \mu^+ \mu^-$ channel. These
 311 q^2 regions are furthest from the charmonium regions and are therefore cleanly predicted

Table 2: Partial branching fractions of $B^0 \rightarrow K^0 \mu^+ \mu^-$ and isospin asymmetries of $B \rightarrow K \mu^+ \mu^-$ decays. The significance of the deviation of A_I from zero is shown in the last column. The errors include the statistical and systematic uncertainties.

q^2 range [GeV ² /c ⁴]	$d\mathcal{B}/dq^2$ [10 ⁻⁸ /GeV ² /c ⁴]	A_I	$\sigma(A_I = 0)$
0.05 – 2.00	$1.1^{+1.4}_{-1.2}$	$-0.55^{+0.40}_{-0.56}$	1.5
2.00 – 4.30	$0.3^{+1.1}_{-0.9}$	$-0.76^{+0.45}_{-0.79}$	1.9
4.30 – 8.68	2.8 ± 0.7	$0.00^{+0.14}_{-0.15}$	0.1
10.09 – 12.86	$1.8^{+0.8}_{-0.7}$	$-0.15^{+0.19}_{-0.22}$	0.8
14.18 – 16.00	$1.1^{+0.7}_{-0.5}$	-0.40 ± 0.22	1.9
16.00 – 23.00	$0.5^{+0.3}_{-0.2}$	$-0.52^{+0.18}_{-0.22}$	3.0
1.00 – 6.00	$1.3^{+0.9}_{-0.7}$	$-0.35^{+0.23}_{-0.27}$	1.7

Table 3: Partial branching fractions of $B^+ \rightarrow K^{*+} \mu^+ \mu^-$ and isospin asymmetries of $B \rightarrow K^* \mu^+ \mu^-$ decays. The significance of the deviation of A_I from zero is shown in the last column. The errors include the statistical and systematic uncertainties.

q^2 range [GeV ² /c ⁴]	$d\mathcal{B}/dq^2$ [10 ⁻⁸ /GeV ² /c ⁴]	A_I	$\sigma(A_I = 0)$
0.05 – 2.00	$7.0^{+3.1}_{-3.0}$	$0.05^{+0.27}_{-0.21}$	0.2
2.00 – 4.30	$5.4^{+2.6}_{-2.4}$	$-0.27^{+0.29}_{-0.18}$	0.9
4.30 – 8.68	$5.7^{+2.0}_{-1.7}$	$-0.06^{+0.19}_{-0.14}$	0.4
10.09 – 12.86	$7.7^{+2.6}_{-2.4}$	$-0.16^{+0.17}_{-0.16}$	0.9
14.18 – 16.00	$5.5^{+2.6}_{-2.1}$	$0.02^{+0.23}_{-0.21}$	0.1
16.00 – 19.30	3.8 ± 1.4	$0.02^{+0.21}_{-0.20}$	0.1
1.00 – 6.00	$5.8^{+1.8}_{-1.7}$	-0.15 ± 0.16	1.0

312 theoretically. This asymmetry is dominated by a deficit in the observed $B^0 \rightarrow K^0 \mu^+ \mu^-$
313 signal. Ignoring the small correlation of errors between each q^2 bin, the significance of
314 the deviation from zero integrated across q^2 is calculated to be 4.4σ . The $B \rightarrow K^* \mu^+ \mu^-$
315 case agrees with the SM prediction of almost zero isospin asymmetry [1]. All results agree
316 with previous measurements [3, 32, 33].

317 Acknowledgements

318 We would like to thank Christoph Bobeth, Danny van Dyk and Gudrun Hiller for provid-
319 ing SM predictions for the branching fractions and the isospin asymmetry of $B \rightarrow K^* \mu^+ \mu^-$
320 decays. We express our gratitude to our colleagues in the CERN accelerator departments
321 for the excellent performance of the LHC. We thank the technical and administrative

322 staff at CERN and at the LHCb institutes, and acknowledge support from the National
323 Agencies: CAPES, CNPq, FAPERJ and FINEP (Brazil); CERN; NSFC (China);
324 CNRS/IN2P3 (France); BMBF, DFG, HGF and MPG (Germany); SFI (Ireland); INFN
325 (Italy); FOM and NWO (The Netherlands); SCSR (Poland); ANCS (Romania); MinES
326 of Russia and Rosatom (Russia); MICINN, XuntaGal and GENCAT (Spain); SNSF and
327 SER (Switzerland); NAS Ukraine (Ukraine); STFC (United Kingdom); NSF (USA). We
328 also acknowledge the support received from the ERC under FP7 and the Region Au-
329 vergne.

330 References

- 331 [1] T. Feldmann and J. Matias, *Forward-backward and isospin asymmetry for $B \rightarrow$*
332 *$K^{(*)}l^+l^-$ decay in the Standard Model and in supersymmetry*, JHEP **01** (2003) 074,
333 [arXiv:hep-ph/0212158](#).
- 334 [2] BaBar collaboration, B. Aubert *et al.*, *Direct CP, lepton flavor and isospin asym-*
335 *metries in the decays $B \rightarrow K^{(*)}l^+l^-$* , Phys. Rev. Lett. **102** (2008) 091803,
336 [arXiv:0807.4119](#).
- 337 [3] Belle collaboration, J.-T. Wei *et al.*, *Measurement of the differential branching frac-*
338 *tion and forward-backward asymmetry for $B \rightarrow K^{(*)}l^+l^-$* , Phys. Rev. Lett. **103** (2009)
339 171801, [arXiv:0904.0770](#).
- 340 [4] Heavy Flavor Averaging Group, D. Asner *et al.*, *Averages of b-hadron, c-hadron, and*
341 *τ -lepton properties*, [arXiv:1010.1589](#).
- 342 [5] LHCb collaboration, A. A. Alves Jr. *et al.*, *The LHCb detector at the LHC*, JINST
343 **3** (2008) S08005.
- 344 [6] V. Gligorov, C. Thomas, and M. Williams, *The HLT inclusive B triggers*, LHCb-
345 PUB-2011-016.
- 346 [7] T. Sjöstrand, S. Mrenna, and P. Skands, *PYTHIA 6.4 Physics and manual*, JHEP
347 **05** (2006) 026, [arXiv:hep-ph/0603175](#).
- 348 [8] I. Belyaev *et al.*, *Handling of the generation of primary events in GAUSS, the LHCb*
349 *simulation framework*, Nuclear Science Symposium Conference Record (NSS/MIC)
350 **IEEE** (2010) 1155.
- 351 [9] D. J. Lange, *The EvtGen particle decay simulation package*, Nucl. Instrum. Meth.
352 **A462** (2001) 152.
- 353 [10] P. Golonka and Z. Was, *PHOTOS Monte Carlo: a precision tool for QED corrections*
354 *in Z and W decays*, Eur. Phys. J. **C45** (2006) 97, [arXiv:hep-ph/0506026](#).

- 355 [11] A. Ali, P. Ball, L. T. Handoko, and G. Hiller, *Comparative study of the decays $B \rightarrow$*
356 *$(K, K^*)\ell^+\ell^-$ in Standard Model and supersymmetric theories*, Phys. Rev. **D61** (2000)
357 074024, [arXiv:hep-ph/9910221](#).
- 358 [12] GEANT4 collaboration, J. Allison *et al.*, *Geant4 developments and applications*,
359 IEEE Trans. Nucl. Sci. **53** (2006) 270; GEANT4 collaboration, S. Agostinelli *et al.*,
360 *GEANT4: A simulation toolkit*, Nucl. Instrum. Meth. **A506** (2003) 250.
- 361 [13] M. Clemencic *et al.*, *The LHCb simulation application, Gauss: design, evolution and*
362 *experience*, J. of Phys: Conf. Ser. **331** (2011) 032023.
- 363 [14] P. Speckmayer, A. Höcker, J. Stelzer, and H. Voss, *The toolkit for multivariate data*
364 *analysis TMVA 4*, J. of Phys: Conf. Ser. **219** (2010) 032057.
- 365 [15] R. Aaij *et al.*, *Differential branching fraction and angular analysis of the decay $B^0 \rightarrow$*
366 *$K^{*0}\mu^+\mu^-$* , Phys. Rev. Lett. **108** (2012) 181806, [arXiv:1112.3515](#).
- 367 [16] T. Skwarnicki, *A study of the radiative cascade transitions between the Upsilon-prime*
368 *and Upsilon resonances*, PhD thesis, Institute of Nuclear Physics, Krakow, 1986,
369 DESY-F31-86-02.
- 370 [17] P. Koppenburg, *Selection of $B^+ \rightarrow llK$ at LHCb and sensitivity to R_K* , LHCb-2007-
371 034.
- 372 [18] K. G. Wilson, *Non-Lagrangian models of current algebra*, Phys. Rev. **179** (1969)
373 1499.
- 374 [19] K. G. Wilson and W. Zimmermann, *Operator product expansions and composite field*
375 *operators in the general framework of quantum field theory*, Commun. Math. Phys.
376 **24** (1972) 87.
- 377 [20] D. Melikhov, B. Stech, *Weak form factors for heavy meson decays: an update*, Phys.
378 Rev. **D62** (2000) 014006, [arXiv:hep-ph/0001113](#).
- 379 [21] Particle Data Group, K. Nakamura *et al.*, *Review of particle physics*, J. Phys. **G37**
380 (2010) 075021.
- 381 [22] C. Bobeth, G. Hiller, and D. van Dyk, *More benefits of semileptonic rare B decays*
382 *at low recoil: CP Violation*, JHEP **07** (2011) 067, [arXiv:1105.0376](#).
- 383 [23] C. Bobeth, G. Hiller, D. van Dyk, and C. Wacker, *The Decay $B \rightarrow K\ell^+\ell^-$ at low*
384 *hadronic recoil and model-independent $\Delta B = 1$ constraints*, JHEP **01** (2012) 107,
385 [arXiv:1111.2558](#).
- 386 [24] Private communication with C. Bobeth, G. Hiller and D. van Dyk.
- 387 [25] M. Beneke, T. Feldmann, and D. Seidel, *Systematic approach to exclusive $B \rightarrow$*
388 *Vl^+l^- , $V\gamma$ decays*, Nucl. Phys. **B612** (2001) 25, [arXiv:hep-ph/0106067](#).

- 389 [26] M. Beneke, T. Feldmann, and D. Seidel, *Exclusive radiative and electroweak*
390 *$b \rightarrow d$ and $b \rightarrow s$ penguin decays at NLO*, Eur. Phys. J. **C41** (2005) 173,
391 arXiv:hep-ph/0412400.
- 392 [27] C. Bobeth, G. Hiller, and G. Piranishvili, *Angular distributions of $\bar{B} \rightarrow K\bar{\ell}\ell$ decays*,
393 JHEP **12** (2007) 040, arXiv:0709.4174.
- 394 [28] B. Grinstein and D. Pirjol, *Exclusive rare $B \rightarrow K^*\ell^+\ell^-$ - decays at low re-*
395 *coil: controlling the long-distance effects*, Phys. Rev. **D70** (2004) 114005,
396 arXiv:hep-ph/0404250.
- 397 [29] P. Ball and R. Zwicky, *$B_{d,s} \rightarrow \rho, \omega, K^*, \phi$ decay form factors from light-cone sum*
398 *rules reexamined*, Phys. Rev. **D71** (2005) 014029, arXiv:hep-ph/0412079.
- 399 [30] A. Khodjamirian, T. Mannel, A. Pivovarov, and Y.-M. Wang, *Charm-loop effect in*
400 *$B \rightarrow K^{(*)}\ell^+\ell^-$ and $B \rightarrow K^*\gamma$* , JHEP **09** (2010) 089, arXiv:1006.4945.
- 401 [31] U. Egede *et al.*, *New observables in the decay mode $\bar{B}_d^0 \rightarrow \bar{K}^{*0}\ell^+\ell^-$* , JHEP **11** (2008)
402 032, arXiv:0807.2589.
- 403 [32] BaBar collaboration, *Measurement of branching fractions and rate asymmetries in*
404 *the rare decays $B \rightarrow K^{(*)}\ell^+\ell^-$* , submitted to Phys. Rev. **D**, arXiv:1204.3933.
- 405 [33] CDF collaboration, T. Aaltonen *et al.*, *Observation of the baryonic flavor-changing*
406 *neutral current decay $\Lambda_b^0 \rightarrow \Lambda\mu^+\mu^-$* , Phys. Rev. Lett. **107** (2011) 201802,
407 arXiv:1107.3753.